SOME ATTEMPTS TO SIMULATE THE DEVELOPMENT OF TROPICAL CYCLONES BY NUMERICAL METHODS

STANLEY L. ROSENTHAL

National Hurricane Research Project, U.S. Weather Bureau, Miami, Fla.

ABSTRACT

The results of a series of numerical experiments which were intended to simulate the *warming* and *developing* stages of hurricane formation are discussed. In the experiments, an initially weak cyclone develops into an intense vortex. However, the deepening proceeds too rapidly and meridional circulations which are too intense develop. The inclusion of ground friction and vertical mixing leads to solutions which are even less acceptable. Lateral mixing slows the development but only provides a temporary delay in the generation of an unacceptably intense meridional circulation.

1. INTRODUCTION

According to Yanai [19], the genesis of hurricanes (typhoons) consists of three distinct stages, the *wave stage*, the *warming stage*, and the *developing stage*. In the *wave stage*, a distinct perturbation, but not a closed vortex, is found in the lower tropospheric easterlies. Ascent occurs in the cold air and the origin of the perturbation-kinetic energy is probably the kinetic energy of the basic current. In the *warming stage*, the temperature rises in the region of ascent and the disturbance becomes warm core. This warming is produced by the release of latent heat in a large number of convective clouds which are embedded in the synoptic-scale circulation. In the *developing stage*, there is a sudden fall of sea level pressure and a rapid generation of large amounts of rotational kinetic energy.

The purpose of this paper is to report on a series of numerical experiments which were intended to simulate the later portions of the *warming stage* and the early aspects of the *developing stage*. To formulate the experiment, it is necessary, at the very least, to have a fairly clear qualitative picture of the physical processes which are to be modeled. The *warming* and *developing stages* are idealized as follows.

We assume the initial state to be a weak, cyclonic vortex which is symmetrical. This vortex is assumed to be stable with respect to dry adiabatic, nonviscous dis-

placements in a meridional plane. The following inequalities must, therefore, be valid (see, for example, [1]).

$$\frac{\partial \Theta}{\partial p} < 0 \tag{i}$$

and

$$\left(\frac{\partial M_a^2}{\partial r}\right)_p > 0 \tag{ii}$$

and

$$\left(\frac{\partial \Theta}{\partial r}\right)_p \left(\frac{\partial M_a^2}{\partial p}\right) - \left(\frac{\partial M_a^2}{\partial r}\right)_p \left(\frac{\partial \Theta}{\partial p}\right) > 0 \tag{iii}$$

where Θ is the potential temperature, p is pressure, r is radial distance, M_a is the absolute angular momentum per unit mass.

$$M_a = rv_\theta + fr^2/2$$

v_θ is the tangential component of the wind and f is the Coriolis parameter.

A large number of convective clouds are embedded in this initial vortex. In each of these clouds, there is pseudo-adiabatic ascent through a conditionally unstable atmosphere. The clouds are organized with respect to the vortex and form a definite cloud system. As postulated by Yanai [19], the cloud system plays two important roles in the intensification of the vortex: (1) it builds a strong warm core and (2) it modifies the lapse rate which is initially conditionally unstable so that it becomes

neutral with respect to pseudo-adiabatic ascent. When the second of these modifications has been completed, the vortex, on the average, is statically stable since regions not included in the cloud system are considered regions of dry descent. At this time, due to increased baroclinicity, the stability criterion (iii) may no longer be valid ($\partial\theta/\partial p$ taken negative). Yanai [19] suggests that if this occurs, the vortex may become unstable with respect to large-scale meridional circulations and that overturning, similar to that of the upper Hadley regime [8], may occur. This initiates the *developing stage*.

Although the release of latent heat and the ascent associated with it occur in individual clouds, it should be possible to treat the net effect of the cloud system as a larger-scale, pseudo-adiabatic ascent. This point of view is generally adopted in empirical studies (see, for example, [13, 14, 15]). However, the concept of a large-scale, pseudo-adiabatic ascent leads to serious difficulties in numerical experiments [5, 18]. The maximum growth rate for pseudo-adiabatic disturbances embedded in a symmetrical vortex occurs at the cloud scale when the atmospheric stratification is conditionally unstable [7, 10, 19]. Furthermore, the growth rates for these small-scale disturbances are extremely large. As a result, though the initial conditions contain only large-scale features, small-scale disturbances which are generated by truncation errors, round-off errors, and nonlinear interactions exhibit rapid growth. In the experiments performed by Kasahara [5] and Syōno [18], the large-scale circulations were completely overwhelmed by the smaller-scale ones in a few hours.

It would, therefore, seem desirable to alter the governing differential equations such that the growth rates of the cloud-scale motions would be substantially reduced. This alteration should not, however, destroy the ability for large-scale, pseudo-adiabatic motion to generate warm cores and neutral lapse rates. Since the instability under discussion is essentially a gravitational one [11], requirement of a balance between the pressure field and the rotational component of the wind should lead to its elimination. Kuo [9] has shown that motion which is in hydro-static and gradient-wind balance cannot exhibit gravitational instability. Utilization of this filter, however, makes it necessary to solve an extremely complicated diagnostic equation at each time step of a numerical integration (see Eliassen [1, 2, 3]). Furthermore, this diagnostic equation becomes hyperbolic when the stability criterion (iii) becomes invalid. This precludes the possibility of continuing the experiment into the *developing stage*. We have, therefore, not adopted the gradient-wind filter.

Kuo [9] and Kasahara [6] have shown that lateral-eddy mixing will decrease the cloud-scale growth rates and shift the maximum growth rate toward the larger scales of motion. Since lateral mixing terms act in a fashion analogous to entrainment, their inclusion in a model is not unreasonable. Kuo [9], however, felt that the coefficient

of eddy viscosity needed to produce the desired effect was much too large to be realistic. Kasahara's model [5] and Syōno's model [18] both contained lateral mixing terms. Apparently, the coefficients were too small to provide significant alterations in the growth-rate spectrum. In a second series of experiments, Kasahara [6] varied the lateral mixing coefficient in a manner such that disturbances of a desired scale were dominant. One of these experiments, carried to about 2 hours of real time, yielded results which seemed fairly reasonable. Our experience, however, indicates that large coefficients of lateral mixing produce a drastic damping of the rotational wind.

In the integrations which we have performed, gravitational instability is controlled, to a certain extent, by truncation error. In any numerical experiment, motions smaller in scale than twice the distance between grid points are automatically eliminated since they cannot be represented on the mesh. The growth-rate spectrum for gravitational instability (see, for example, [9, 11]) shows that growth rates decrease rapidly as the scale increases beyond the scale of maximum growth rate. This suggests that intensification due to gravitational instability may be controlled by adoption of a coarse radial mesh. By use of a radial increment of 40 km., we have eliminated disturbances with scales less than 80 km. Although the physical significance of this procedure is not clear, it would seem that the approach taken is related to the utilization of a coefficient of lateral mixing whose magnitude is dependent on scale. For scales less than 80 km., the lateral mixing coefficient would be considered infinite. At a scale of 80 km., the coefficient is imagined to be of moderate magnitude. The coefficient is envisioned to decrease rapidly as the scale increases beyond 80 km.

Based on the integrations performed by Kasahara [5] and Syōno [18] and on the various linear analyses which are available [6, 7, 9, 10, 19], one would expect the dominant scale in this system to be near 80 km. if the initial state is barotropic. If baroclinicity is present and if the growth rate for gravitational instability at a scale of 80 km. is relatively small, one might expect the dominant disturbance to have a scale in excess of 80 km. The numerical integrations discussed in section 6 indicate that the dominant mode occurs at a scale significantly greater than 80 km. In essence, the coarse radial increment eliminates the enormous growth rates due to gravitational instability on a small scale which were present in the calculations performed by Kasahara [5] and Syōno [18]. The larger-scale disturbances are, therefore, allowed to develop without being overwhelmed by the smaller-scale ones.

This approach, though arbitrary, produces the desired result. As stated earlier, we wish to include the net effect of the cloud system but not the individual clouds. The cloud system varies more slowly and has a net ascent which is far less than that of individual clouds. In effect, we treat the cloud system as an enormous, slowly varying, moderately intense cloud.

2. THE BASIC EQUATIONS

The equations which govern circularly symmetrical flow in a hydrostatic atmosphere are:

$$\frac{\partial v_\theta}{\partial t}=-v_r\frac{\partial v_\theta}{\partial r}-w\frac{\partial v_\theta}{\partial z}-v_r\left(f+\frac{v_\theta}{r}\right)+F_\theta, \tag{1}$$

$$\frac{\partial v_r}{\partial t}=-v_r\frac{\partial v_r}{\partial r}-w\frac{\partial v_r}{\partial z}+v_\theta\left(f+\frac{v_\theta}{r}\right)-\frac{1}{\rho}\frac{\partial p}{\partial r}+F_r, \tag{2}$$

$$\frac{\partial p}{\partial z}=-\rho g, \tag{3}$$

$$\frac{\partial \Theta}{\partial t}=-v_r\frac{\partial \Theta}{\partial r}-w\frac{\partial \Theta}{\partial z}+\frac{\Theta}{c_p T}H, \tag{4}$$

$$\Theta=T\left(\frac{p_0}{p}\right)^{R/c_p}, \tag{5}$$

$$p=\rho RT, \tag{6}$$

and

$$\frac{\partial \rho}{\partial t}+\frac{\partial \rho v_r}{\partial r}+\frac{\rho v_r}{r}+\frac{\partial \rho w}{\partial z}=0. \tag{7}$$

The symbols are defined as follows:

v_θ tangential component of the wind
v_r radial component of the wind
w vertical velocity of the air
t time
r radial coordinate
z height
f Coriolis parameter (assumed constant)
F_θ tangential component of the viscous force per unit mass
F_r radial component of the viscous force per unit mass
ρ air density
p air pressure
g acceleration of apparent gravity
Θ potential temperature
H heat added to air per unit mass and time
c_p specific heat capacity at constant pressure for dry air
p_0 1000 mb.
R specific gas constant for dry air
T air temperature

For F_θ and F_r, we assume

$$F_\theta=\frac{1}{\rho_s}\frac{\partial}{\partial z}\left(\rho_s K_z\frac{\partial v_\theta}{\partial z}\right)+K_H\frac{\partial}{\partial r}\left(\frac{\partial v_\theta}{\partial r}+\frac{v_\theta}{r}\right), \tag{8}$$

$$F_r=\frac{1}{\rho_s}\frac{\partial}{\partial z}\left(\rho_s K_z\frac{\partial v_r}{\partial z}\right)+K_H\frac{\partial}{\partial r}\left(\frac{\partial v_r}{\partial r}+\frac{v_r}{r}\right) \tag{9}$$

where $\rho_s=$ the density of the mean tropical atmosphere, $K_z=$ the kinematic coefficient of eddy viscosity for vertical mixing (at most a function of height), and $K_H=$ the kine-matic coefficient of eddy viscosity for lateral mixing (a constant).

The heating function, H, is assumed to result from pseudo-adiabatic release of latent heat in ascending air and from eddy diffusivity. Therefore,

$$H=\frac{c_p}{\rho_s}\frac{\partial}{\partial z}\left(\rho_s K_z\frac{\partial \Theta}{\partial z}\right)+\frac{c_p K_H}{r}\frac{\partial}{\partial r}\left(r\frac{\partial \Theta}{\partial r}\right)-\gamma Lw\frac{\partial q_s}{\partial z} \tag{10}$$

where $L=$ the latent heat of vaporization for water substance, $q_s=$ the saturation specific humidity of the mean tropical atmosphere, and $\gamma=1$ for ascent, 0 for descent. Note that the coefficients of eddy viscosity and diffusivity have been assumed equal. Also, we neglect changes of phase other than the condensation of water vapor; fusion and sublimation are not allowed. Finally, all ascending air is assumed saturated with water vapor. This eliminates the need to include an equation of continuity for water vapor.

The relative angular momentum per unit mass is given by

$$M=rv_\theta. \tag{11}$$

Let the function ϕ be defined by

$$\phi=c_p\left(\frac{p}{p_0}\right)^{R/c_p}=\frac{c_p T}{\Theta}. \tag{12}$$

Equations (8), (9), (10), (11), and (12) allow us to write (1), (2), (3), and (4), respectively, as

$$\frac{\partial M}{\partial t}=-v_r\frac{\partial M}{\partial r}-w\frac{\partial M}{\partial z}-frv_r+\frac{1}{\rho_s}\frac{\partial}{\partial z}\left(\rho_s K_z\frac{\partial M}{\partial z}\right)$$
$$+\frac{K_H}{r}\frac{\partial}{\partial r}\left(r\frac{\partial M}{\partial r}-2M\right) \tag{13}$$

$$\frac{\partial v_r}{\partial t}=-v_r\frac{\partial v_r}{\partial r}-w\frac{\partial v_r}{\partial z}+\frac{M}{r}\left(f+\frac{M}{r^2}\right)+\frac{1}{\rho_s}\frac{\partial}{\partial z}\left(\rho_s K_z\frac{\partial v_r}{\partial z}\right)$$
$$+K_H\frac{\partial}{\partial r}\left(r\frac{\partial v_r}{\partial r}-2v_r\right)-\Theta\frac{\partial \phi}{\partial r} \tag{14}$$

$$\frac{\partial \phi}{\partial z}=-g/\Theta \tag{15}$$

$$\frac{\partial \Theta}{\partial t}=-v_r\frac{\partial \Theta}{\partial r}-w\left(\frac{\partial \Theta}{\partial z}+\frac{\gamma L}{\phi}\frac{\partial q_s}{\partial z}\right)$$
$$+\frac{c_p}{\rho_s\phi}\frac{\partial}{\partial z}\left(\rho_s K_z\frac{\partial \Theta}{\partial z}\right)+\frac{c_p K_H}{\phi r}\frac{\partial}{\partial r}\left(r\frac{\partial \Theta}{\partial r}\right) \tag{16}$$

Equation (7) is simplified to read

$$\frac{\partial \rho_s v_r}{\partial r}+\frac{\rho_s v_r}{r}+\frac{\partial \rho_s w}{\partial z}=0 \tag{17}$$

or

$$v_r=-\frac{1}{\rho_s r}\frac{\partial \psi}{\partial z} \tag{18a}$$

$$w=\frac{1}{\rho_s r}\frac{\partial \psi}{\partial r} \tag{18b}$$

where ψ is the Stokes stream function. Equation (14) is multiplied by $\rho_s r$ and then differentiated with respect to z. By use of (18a), this sequence of operations yields

$$\frac{\partial^2}{\partial z^2}\left(\frac{\partial \psi}{\partial t}\right)=-\frac{\partial(\rho_s r \Gamma)}{\partial z}+\frac{\partial}{\partial z}\left(\rho_s \Theta r\frac{\partial \phi}{\partial r}\right) \tag{19}$$

where

$$\rho_s r\Gamma=\frac{\partial}{\partial z}\left(\rho_s K_z\frac{\partial rv_r}{\partial z}\right)+\frac{\rho_s K_H}{r}\frac{\partial}{\partial r}\left(r\frac{\partial rv_r}{\partial r}-2rv_r\right)$$
$$+\rho_s M\left(f+\frac{M}{r^2}\right)-\rho_s r\left(v_r\frac{\partial v_r}{\partial r}+w\frac{\partial v_r}{\partial z}\right). \tag{20}$$

Equations (13), (15), (16), (18a), (18b), and (19), together with suitable boundary conditions, form a closed mathematical system for the dependent variables, M, Θ, ϕ, v_r, w, and ψ.

3. BOUNDARY CONDITIONS

We treat the air enclosed in a cylinder of radius 1000 km. which is bounded vertically by mean sea level and the 100-mb. surface. The latter is considered level and rigid (an analog to the tropical tropopause). From the kinematic boundary condition,

$$w_{z=0}=0 \tag{21}$$

$$w_{z=h}=0 \tag{22}$$

where h is the 100-mb. height. To isolate the system, v_r is set to zero at the outer radius. Since the system is closed and symmetrical, the curve, $r=0$, $z=0$, $r=1000$ km., $z=h$, in any meridional cross-section, must be a streamline. This is achieved by the requirements,

$$\psi=0 \tag{23}$$

$$\frac{\partial \psi}{\partial t}=0 \tag{24}$$

for $r=0$, $r=1000$ km., $z=0$, $z=h$.

In addition to (21), (22), (23), and (24), the following conditions are also imposed:

$$\left(\rho_s K_z\frac{\partial M}{\partial z}\right)_{z=0}=C_D(\rho_s|v_\theta|M)_{z=0} \tag{25}$$

$$\left(\rho_s K_z\frac{\partial rv_r}{\partial z}\right)_{z=0}=C_D(\rho_s|v_\theta|rv_r)_{z=0} \tag{26}$$

$$\left(c_p\rho_s K_z\frac{\partial \Theta}{\partial z}\right)_{z=0}=C_D[\rho_s|v_\theta|c_p(T-T_{\text{sea}})]_{z=0} \tag{27}$$

$$\left(\rho_s K_z\frac{\partial M}{\partial z}\right)_{z=h}=0 \tag{28}$$

$$\left(\rho_s K_z\frac{\partial rv_r}{\partial z}\right)_{z=h}=0 \tag{29}$$

$$(T-T_s)_{z=h}=0 \tag{30}$$

$$\left[\frac{\partial}{\partial z}(T-T_s)\right]_{z=h}=0 \tag{31}$$

$$\left[\frac{\partial}{\partial r}\left(r\frac{\partial \Theta}{\partial r}\right)\right]_{r=1000\text{ km.}}=0 \tag{32}$$

$$\left[\frac{\partial}{\partial r}\left(r\frac{\partial M}{\partial r}-2M\right)\right]_{r=1000\text{ km.}}=0. \tag{33}$$

C_D is the drag coefficient (assumed constant); T_{sea} is the temperature of the sea surface (also assumed constant); T_s is the temperature of the mean tropical atmosphere. Equations (30) and (31) require that the departure of the temperature from mean tropical conditions must vanish at the upper boundary such that the actual sounding becomes tangent to the mean sounding. By use of (3), (5), (6), (30), and (31), it may be shown that

$$\left(c_p\rho_s K_z\frac{\partial \Theta}{\partial z}\right)_{z=h}=\left[\frac{\rho_s K_z\Theta_s}{T_s}\left(\frac{\partial T_s}{\partial z}-\frac{g}{c_p}\right)\right]_{z=h}. \tag{34}$$

Finally, the conditions

$$\left(\frac{\partial \phi}{\partial r}\right)_{r=0}=0 \tag{35}$$

$$\left(\frac{\partial \Theta}{\partial r}\right)_{r=0}=0 \tag{36}$$

are imposed. Section 5 will show the manner in which the conditions listed above enter the numerical calculation.

4. INITIAL CONDITIONS

We assume the initial temperature to be given as a function of r and z. The hydrostatic equation is then integrated downward from the 100-mb. surface to obtain the initial pressure field. The tangential wind, at the initial instant, is assumed to be in gradient balance. It may, therefore, be calculated directly from the temperature and pressure fields.

All that need now be established is the initial distribution of ψ. This is obtained from a diagnostic scheme first presented by Eliassen [1, 2, 3] and recently applied to tropical cyclones by Estoque [4]. Our adaptation of this procedure is discussed elsewhere [17].

5. FINITE-DIFFERENCE EQUATIONS

A rectangular grid, consisting of 31 points (rows) in the vertical direction spaced at 550-m. intervals and 26 points (columns) in the radial direction spaced at 40-km. intervals, was adopted. Forward time differences were used. To maintain computational stability, space derivatives in advective terms were calculated from noncentered, upstream differences. This is the Lelevier (see [16]) scheme which Kasahara [5, 6] also employed. This differencing scheme is a damping one [12]. Short-wave components are damped most heavily [12].

To start the computation, ψ is forecast from the difference analog to (19). In view of (23) and (24), equation

(19) is applied only to interior-grid points. $(\partial/\partial z)(\rho_s r\Gamma)$ and $(\partial/\partial z)(\rho_s\Theta\partial\phi/\partial r)$ are calculated from centered differences over a double height increment with $\partial\phi/\partial r$ evaluated by a centered difference over a double radial increment. $\rho_s r\Gamma$ must be calculated at all grid points with the exception of those which fall along $r=0$ and $r=1000$ km. The advection terms in $\rho_s r\Gamma$ are evaluated by noncentered, upstream differences over a single grid interval. The rotational terms in $\rho_s r\Gamma$ are obtained directly from the point values of ρ_s, r, and M.

$(\partial/\partial z)(\rho_s K_z\partial rv_r/\partial z)$, at interior-grid points, is computed from

$$\left[\frac{\partial}{\partial z}\left(\rho_s K_z\frac{\partial rv_r}{\partial z}\right)\right]_i=\frac{[(\rho_s K_z)_{i+1}+(\rho_s K_z)_i][(rv_r)_{i+1}-(rv_r)_i]}{2(\Delta z)^2}$$
$$-\frac{[(\rho_s K_z)_i+(\rho_s K_z)_{i-1}][(rv_r)_i-(rv_r)_{i-1}]}{2(\Delta z)^2} \quad (37)$$

where i is the row index. Equation (37) represents an extension of Richtmyer's [16; p. 93] method 1 for computing diffusion terms. At the upper and lower boundaries, respectively,

$$\left[\frac{\partial}{\partial z}\left(\rho_s K_z\frac{\partial rv_r}{\partial z}\right)\right]_{30}=\frac{2}{\Delta z}\left\{\left(\rho_s K_z\frac{\partial rv_r}{\partial z}\right)_{30}\right.$$
$$\left.-\frac{[(\rho_s K_z)_{30}+(\rho_s K_z)_{29}][(rv_r)_{30}-(rv_r)_{29}]}{2\Delta z}\right\} \quad (38)$$

and

$$\left[\frac{\partial}{\partial z}\left(\rho_s K_z\frac{\partial rv_r}{\partial z}\right)\right]_0=\frac{2}{\Delta z}\left\{\frac{[(\rho_s K_z)_1+(\rho_s K_z)_0][(rv_r)_1-(rv_r)_0]}{2\Delta z}\right.$$
$$\left.-\left(\rho_s K_z\frac{\partial rv_r}{\partial z}\right)_0\right\}. \quad (39)$$

$(\rho_s K_z\partial rv_r/\partial z)_{30}$ and $(\rho_s K_z\partial rv_r/\partial z)_0$ are evaluated, respectively, from equations (29) and (26).

The contribution to $\rho_s r\Gamma$ by lateral mixing may be written

$$\frac{\rho_s K_H}{r}\frac{\partial}{\partial r}\left(r\frac{\partial rv_r}{\partial r}\right)-\frac{2\rho_s K_H}{r}\frac{\partial rv_r}{\partial r}. \quad (40)$$

The first term is treated in a fashion analogous to that of the vertical mixing term. Since $\rho_s r\Gamma$ is not calculated at $r=0$ and $r=1000$ km., no special conditions on the lateral mixing terms are needed. The second term in (40) has the form of a radial advection by a positive v_r. It is, therefore, evaluated by a noncentered, inward difference over a single radial interval.

After calculation of the right side of (19), $(\partial^2/\partial z^2)$ $(\partial\psi/\partial t)$ is written

$$\frac{\left(\frac{\partial\psi}{\partial t}\right)_{i+1}+\left(\frac{\partial\psi}{\partial t}\right)_{i-1}-2\left(\frac{\partial\psi}{\partial t}\right)_i}{(\Delta z)^2}$$

and the resulting difference equation is solved along each column for $(\partial\psi/\partial t)_i$ subject to the conditions, $(\partial\psi/\partial t)_0=$ $(\partial\psi/\partial t)_{30}=0$. A simple, noniterative method given by Richtmyer [16; p. 102] is used for this purpose. The ψ-forecast is completed by writing

$$\psi^{(n+1)}=\psi^{(n)}+\Delta t\left(\frac{\partial\psi}{\partial t}\right)^{(n)} \quad (41)$$

where the superscript (n) denotes the time step. At internal grid points, $v_r^{(n+1)}$ and $w^{(n+1)}$ are obtained from (18a) and (18b) by use of centered differences over a double space increment. At the upper and lower boundaries, $v_r^{(n+1)}$ is calculated from noncentered, inward differences over one height increment. At $r=1000$ km., $w^{(n+1)}$ is calculated from a noncentered, inward difference over one radial increment. To calculate w at $r=0$, we note

$$\lim_{r\to 0}\left(\frac{\partial\psi}{\partial r}\right)=\lim_{r\to 0}(\rho_s rw)=0.$$

Therefore,

$$w_{r=0}=\lim_{r\to 0}\left(\frac{1}{\rho_s r}\frac{\partial\psi}{\partial r}\right)=\frac{1}{\rho_s}\left(\frac{\partial^2\psi}{\partial r^2}\right)_{r=0}. \quad (42)$$

In view of (42) and the symmetry of the motion, an appropriate expression for $w^{(n+1)}$ at $r=0$ is

$$w_{r=0}^{(n+1)}=\frac{2}{\rho_s(\Delta r)^2}[\psi_{r=\Delta r}^{(n+1)}-\psi_{r=0}^{(n+1)}]. \quad (43)$$

Since, at internal grid points, w is calculated from a centered difference over $2\Delta r$, the smallest-scale perturbation which can appear in the w-field has wavelength $3\Delta r$.

When the calculation of $\psi^{(n+1)}$, $v_r^{(n+1)}$, and $w^{(n+1)}$ has been completed, $M^{(n+1)}$ is obtained from the difference analog to (13). The advective terms are calculated from $v_r^{(n+1)}$, $w^{(n+1)}$, and $M^{(n)}$. Again, noncentered, upstream differences over a single space increment are used. $v_r^{(n+1)}$ is used in the calculation of the Coriolis term. The viscous terms in equation (13) are calculated from finite difference expressions which are similar to those used in the computation of $\rho_s r\Gamma$. Equations (25) and (28) are used in the evaluation of the vertical mixing term at the lower and upper boundaries respectively. At $r=0$, all terms in equation (13) vanish. However, at $r=1000$ km., the lateral mixing term must be evaluated and equation (33) is used for this purpose. $M^{(n+1)}$ is obtained from

$$M^{(n+1)}=M^{(n)}+\Delta t\left(\frac{\partial M}{\partial t}\right)^{(n)}. \quad (44)$$

With the exceptions noted below, the finite-difference treatment of equation (16) is identical to that of equation (13). At $z=0$ $(z=h)$, equation (27) (equation 34) is employed in the calculation of the vertical mixing term. At $r=1000$ km., the lateral mixing term is given by equation (32). For $r=0$

$$\lim_{r \to 0} \left[\frac{1}{r} \frac{\partial}{\partial r} \left(r \frac{\partial \Theta}{\partial r} \right) \right] = \lim_{r \to 0} \left[\frac{\partial^2 \Theta}{\partial r^2} + \frac{1}{r} \frac{\partial \Theta}{\partial r} \right]. \tag{45}$$

From equations (36) and (45), we obtain

$$\lim_{r \to 0} \left[\frac{1}{r} \frac{\partial}{\partial r} \left(r \frac{\partial \Theta}{\partial r} \right) \right] = 2 \left(\frac{\partial^2 \Theta}{\partial r^2} \right)_{r=0}. \tag{46}$$

In view of the symmetry of system,

$$\lim_{r \to 0} \left[\frac{1}{r} \frac{\partial}{\partial r} \left(r \frac{\partial \Theta}{\partial r} \right) \right] \approx \frac{4}{(\Delta r)^2} [\Theta_{r=\Delta r} - \Theta_{r=0}]. \tag{47}$$

Finally,

$$\Theta^{(n+1)} = \Theta^{(n)} + \Delta t \left(\frac{\partial \Theta}{\partial t} \right)^{(n)}. \tag{48}$$

$\phi^{(n+1)}$ is calculated from a trapezoidal integration of (15) which progresses downward from the upper boundary (assumed to have a uniform pressure of 100 mb.). Since the time variations of ϕ are not calculated directly from the equation of continuity, the radial average of the sea level pressure (a measure of the total mass of the system) is not conserved. This inconsistency stems directly from the combined effect of the hydrostatic assumption and the neglect of $\partial \rho / \partial t$ in the continuity equation.

The requirement that the system of difference equations described above be computationally stable with respect to linear processes leads to essentially the same criterion as that given by Kasahara [5]. For a radial increment of 40 km. and with allowance for radial winds as strong as 60 m. sec.$^{-1}$ (not to be expected, of course, in a real hurricane), we find that Δt should be no longer than about 200 sec. In actuality, a Δt of 2 min. was used which provides for some degree of computational damping.

6. RESULTS

The initial temperature field (fig. 1a) was taken to resemble that of a weak, warm-core tropical cyclone. The largest departure from mean tropical conditions is 2.4°C. The largest value of $\partial T / \partial r$, about 0.5° C. per 100 km., occurs in the upper troposphere at a radius of about 150 km. The sea level pressure profile (fig. 1b) shows the central pressure of the vortex to be about 1000 mb. The initial tangential (gradient) wind (fig. 2a) is strongest, about 15 m. sec.$^{-1}$, at a radius slightly larger than 200 km. Figures 1c and 1d show, respectively, the initial dry static stability ($\partial \Theta / \partial z$) and wet static stability ($\partial \Theta / \partial z$) + ($L/\phi$) ($\partial q_s / \partial z$).

The initial meridional circulation (figs. 2b, 2c, and 2d) was obtained as described in section 4 and in [17]. The meridional circulation shown by figure 2 is that obtained in Experiment II of [17]. The appropriate parameters are $K_H = 0$, $C_D = 2.5 \times 10^{-1}$, $f = 5 \times 10^{-5}$ sec.$^{-1}$ (20° N.), $T_{sea} = 299.4°$ K. (the same value as the initial sea level air temperature). K_z is 10 m.^{2} sec.$^{-1}$ at $z=0$, zero at $z=h$, and varies linearly between these levels.

The calculations described below were performed on the G.E. 225 computer at the National Hurricane Center. Since internal storage is limited in this computer, diagnostic calculations of ψ are extremely expensive (about the same cost as a 24-hr. integration of the prognostic model). For reasons of economy, the same initial meridional circulation (that shown in figs. 2b, 2c, and 2d) was employed in all experiments despite the fact that various parameters were varied from the values given in the preceding paragraph.

The initial conditions shown by figures 1 and 2 satisfy the stability criteria (i), (ii), and (iii). Hence, if a nonviscous, dry adiabatic integration were to be performed, we would expect the solution to exhibit stable oscillations. As an experimental control, we performed such an intergration ($\gamma = 0$, $K_H = 0$, $K_z = 0$, $C_D = 0$). It is designated as Experiment I. The evolution of the meridional streamlines is shown by figure 3.

The oscillatory nature of the motion is clear. We note, especially in the upper troposphere, the presence of large-scale, rapidly moving inertia-gravity disturbances. Figures 4 and 5 show the evolution of the radial and vertical velocities. The average intensity of the system does not change significantly with time. The tangential wind (not reproduced here) showed little time variation except in the region of highest v_θ. In response to the initial low-level inflow, tangential winds as large as 22 m. sec.$^{-1}$ are found after one hour. However, as the low-level radial motion reverses itself, the values of v_θ tend toward their original values. During the course of the integration, the sea level pressure at $r=0$ oscillates between 999 mb. and 1001 mb.

In Experiment II, $K_H = 0$, $K_z = 0$, and $C_D = 0$, but latent heat is released according to the rules described in section 2. The results of Experiment II are shown by figures 6–10. After two hours (fig. 6), a ring of subsidence surrounds the vortex center (fig. 6a). A similar phenomenon was noted in all integrations which included condensation heating. The two maxima of descent (fig. 6a) are separated by 200 km. ($5\Delta r$). Maximum ascent is 18 cm. sec.$^{-1}$. The horizontal area over which ascent prevails is considerably narrower than it was initially. In the lower levels, the radial velocities (fig. 6b) show no significant changes at radii greater than 200 km. Inward of 200 km., however, outflow has replaced inflow. This is consistent with the subsidence which has developed at the vortex center. Aloft, close to the center, inflow, which feeds the descending current, is found. Warming, due to the release of latent heat in the ascending air, is clearly shown in the temperature field (fig. 6c). At sea level, cooling has occurred in response to adiabatic inflow. By two hours, the central pressure (fig. 10) has decreased to 998 mb. This deepening has been produced by dry adiabatic subsidence near the vortex center. The tangential winds (fig. 6d) have strengthened in the low layers. The maximum v_θ is now 22.5 m. sec.$^{-1}$ as compared to 15.3 initially. Some

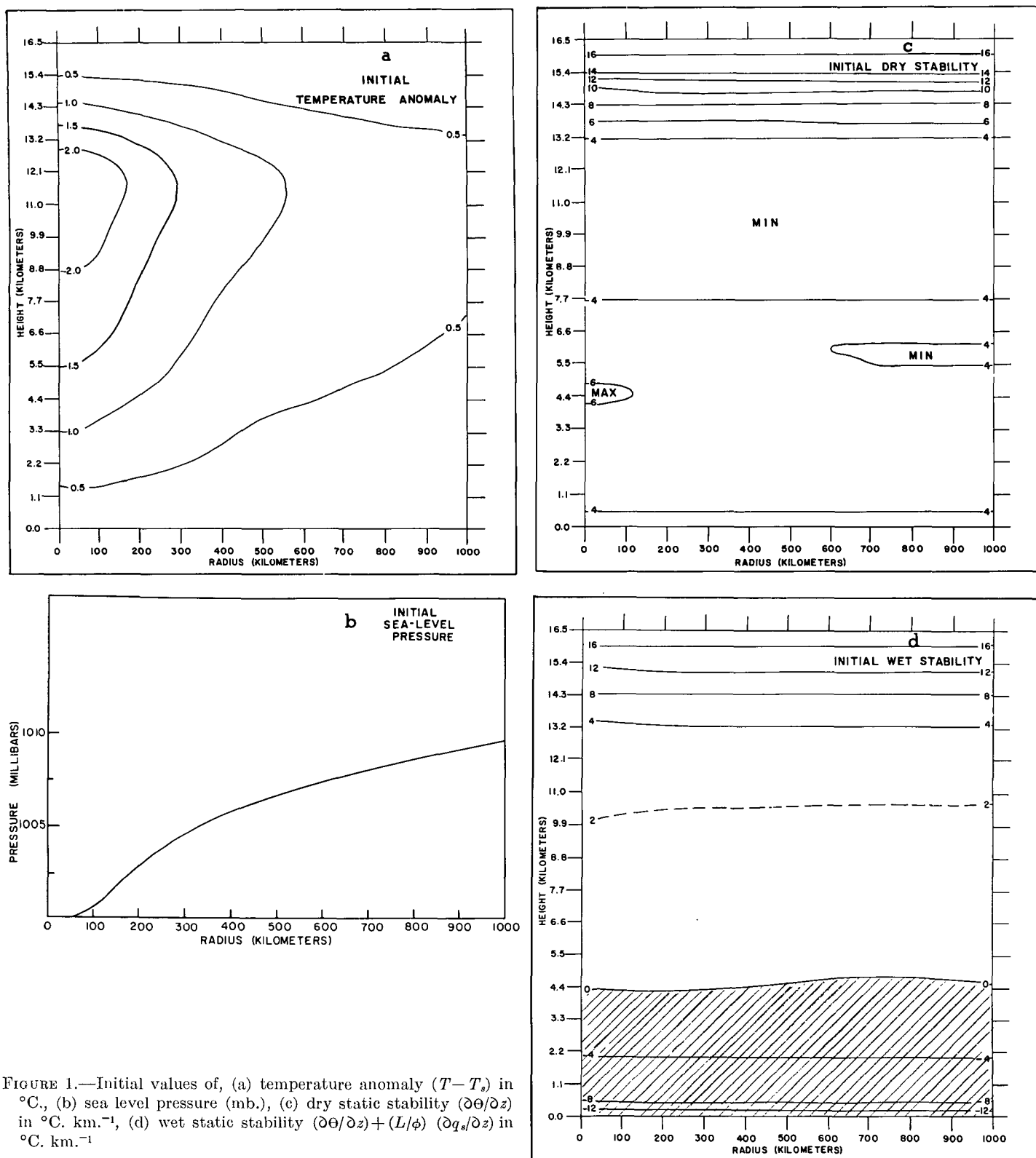FIGURE 1.—Initial values of, (a) temperature anomaly $(T-T_s)$ in °C., (b) sea level pressure (mb.), (c) dry static stability $(\partial\theta/\partial z)$ in °C. km.$^{-1}$, (d) wet static stability $(\partial\theta/\partial z)+(L/\phi)$ $(\partial q_s/\partial z)$ in °C. km.$^{-1}$

patches of negative v_θ appear in the upper troposphere. These are produced by outflow at constant absolute angular momentum and, to a much lesser degree, by truncation error.

By four hours, the width of the main ascending current (fig. 7a) has become even smaller. However, the distance between the two maxima of subsidence remains 200 km. The maximum upward motion is 96 cm. sec.$^{-1}$ Low-level
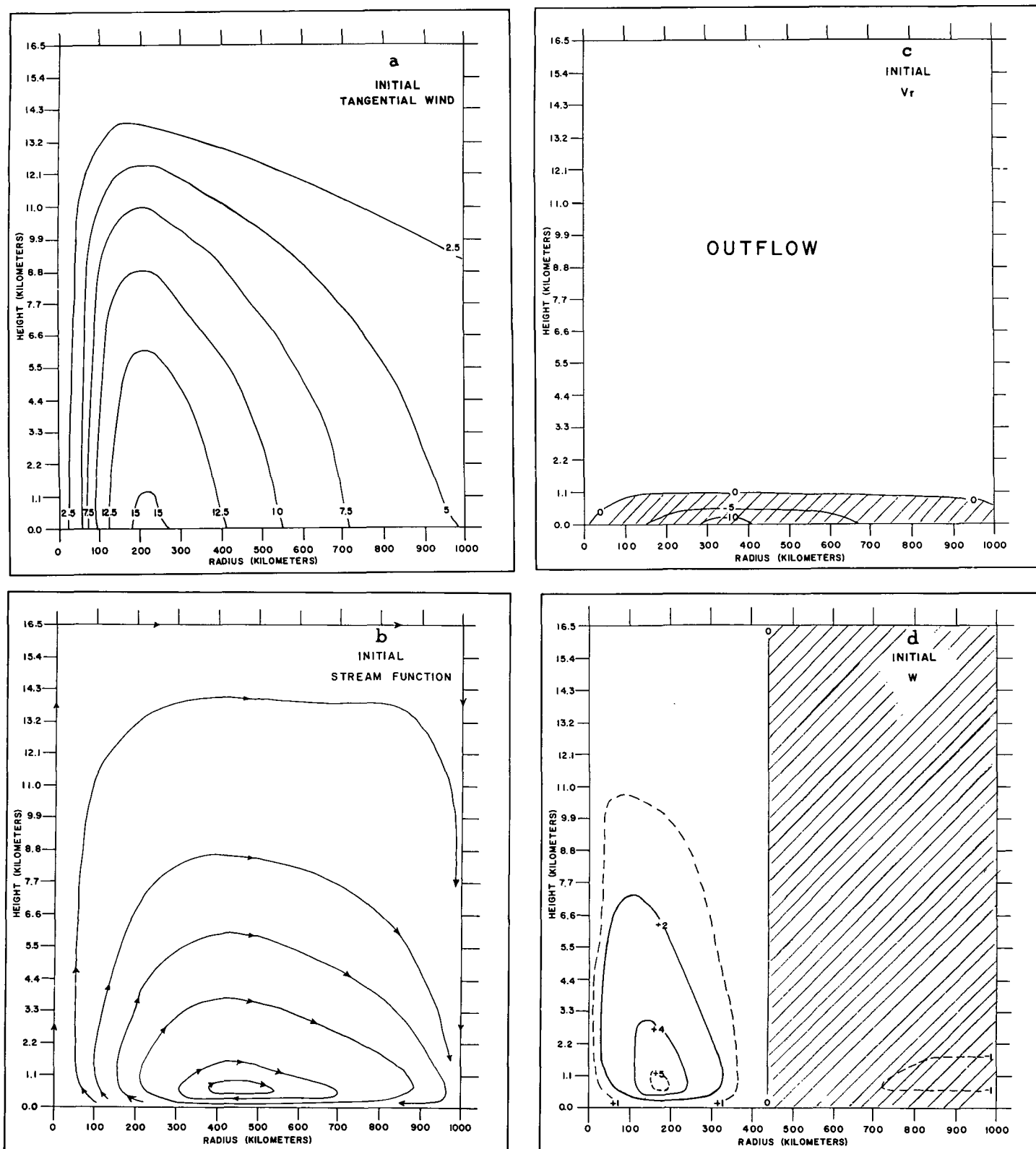
FIGURE 2.—Initial, (a) tangential wind (m. sec.$^{-1}$), (b) meridional streamlines (spacing of streamlines not proportional to speed), (c) radial velocity (m. sec.$^{-1}$), (d) vertical velocity (cm. sec.$^{-1}$)
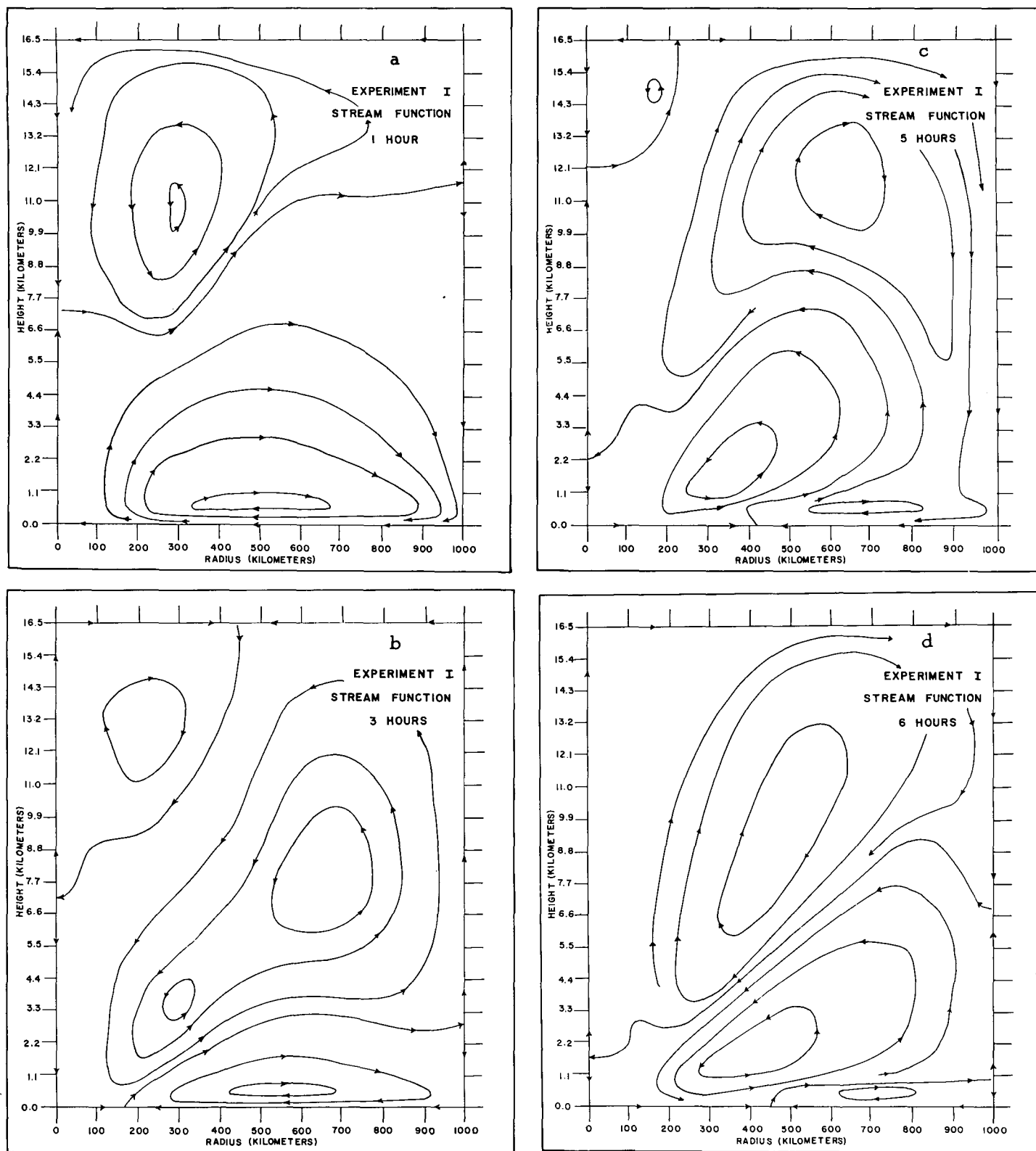
FIGURE 3.—Experiment I, meridional streamlines (spacing not proportional to speed), (a) one hour, (b) three hours, (c) five hours, (d) six hours.
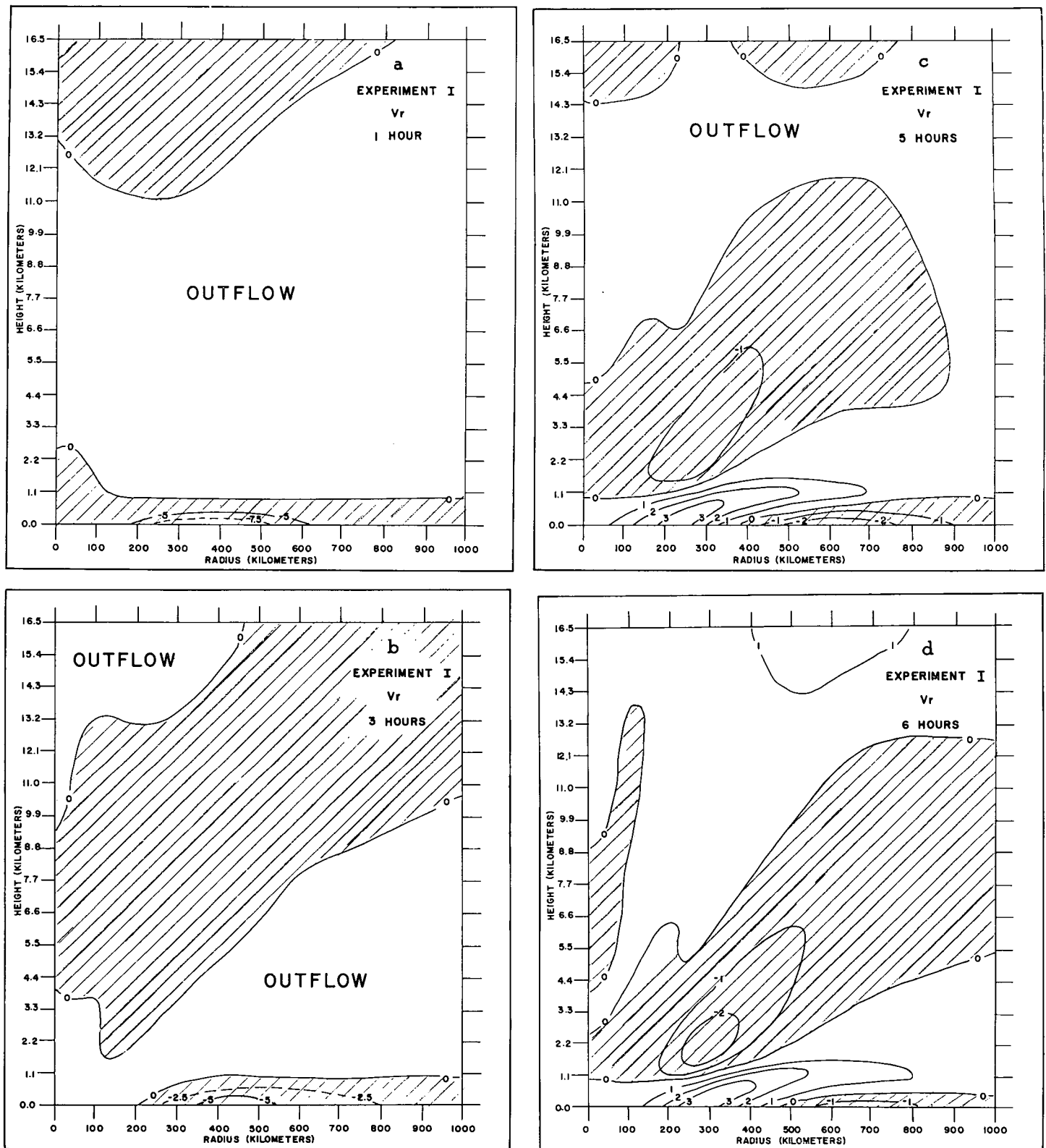
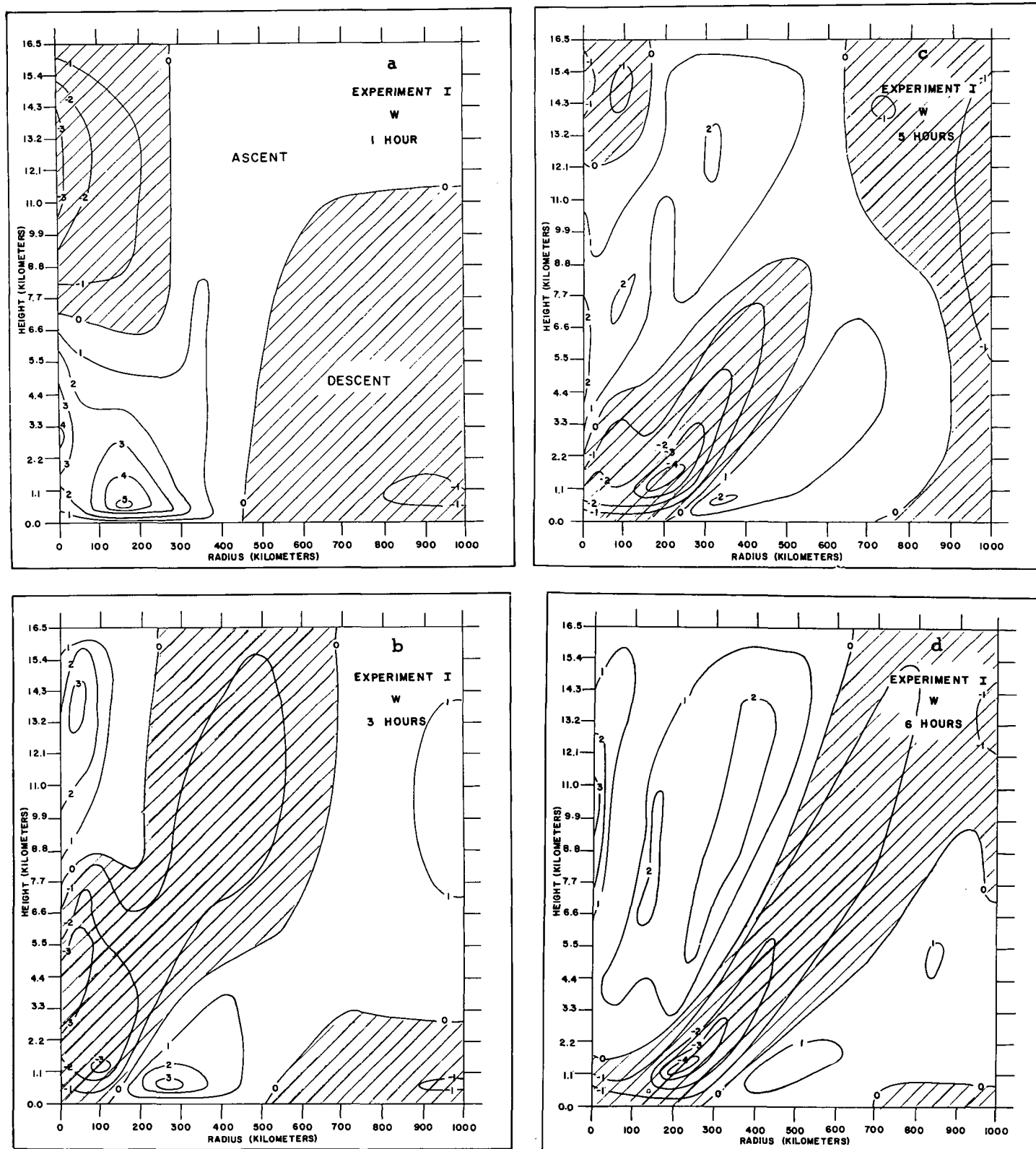FIGURE 4.—Experiment I, radial velocities (m. sec.⁻¹), (a) one hour, (b) three hours, (c) five hours, (d) six hours.

FIGURE 5.—Experiment I, vertical velocities (cm. sec.$^{-1}$), (a) one hour, (b) three hours, (c) five hours, (d) six hours.

descent, near the vortex center, has become as strong as 38 cm. sec.$^{-1}$ The low-level radial velocities (fig. 7b) have strengthened considerably. Extremely strong, low-level convergence is found near a radius of 180 km. In response to the pseudo-adiabatic ascent, lower tropospheric temperature anomalies have increased markedly (fig. 7c). Values as high as 10°C. occur. Aloft, we find cooling which is produced by ascent with absolute static stability. At the vortex center, subsidence has produced marked temperature rises. Close to sea level, adiabatic inflow continues to maintain a shallow layer of cool air. On the whole, horizontal temperature gradients are much stronger at four hours than at the initial instant. Disturbances, with wavelength $2\Delta r$, are now clearly present in the temperature field. They are not, however, the dominant disturbances. The sea level pressure profile (fig. 10) also shows a small-amplitude, $2\Delta r$ component. The central pressure at four hours is 992 mb. and the lowest pressure is 990 mb. The largest value of v_θ (fig. 7d) is now 33.5 m. sec.$^{-1}$ This is about twice the initial value. In the high troposphere, the layer of negative v_θ has continued to develop.

After six hours, the upward vertical motions (fig. 8a) are still stronger. The largest positive w is 295 cm. sec.$^{-1}$ The subsidence close to the vortex center has also intensified; descent as strong as 90 cm. sec.$^{-1}$ is present. A significant feature is the increase in the width of the ascending current which has occurred between four and six hours. The distance between the two centers of maximum descent is now 320 km. ($8\Delta r$). Soundings through the ascending air (not reproduced here) show the lapse rate to be very nearly the process lapse rate except in the low layers where some conditional instability is still present. In the high troposphere, some absolute stability still prevails.

The increase in scale of the vertical motion pattern is, therefore, a reflection of the decreased gravitational instability coupled with a simultaneous increase in the baroclinicity (fig. 8c). Also of importance is a decrease in the rotational stability evidenced by increasing anticyclonic shear in the low levels and increasing anticyclonic rotation in the upper levels (fig. 8d). Despite a moderate loss of M_a due to truncation error, M_a is nowhere negative in the results which we have obtained. Hence, the criterion for rotational stability becomes,

$$\left(\frac{\partial M_a}{\partial r}\right)_p = \left[\left(\frac{\partial v_\theta}{\partial r}\right)_p + \frac{v_\theta}{r} + f\right] r > 0;$$

By six hours, the depth of the low-level inflow (fig. 8b) has markedly increased. The radial velocities have become quite strong. Aloft, outflow values reach 34 m. sec.$^{-1}$ Temperature anomalies (fig. 8c) have increased substantially and, as noted earlier, the radial temperature gradient is quite strong. Aloft, we find continued cooling due to the ascent of statically stable air. The maximum tangential velocity (fig. 8d) is 44 m. sec.$^{-1}$ The upper

level region of negative v_θ has become thicker and more intense. As noted earlier, strong anticyclonic shears have developed in the lower troposphere. The sea level pressure profile (fig. 10), the temperature anomalies (fig. 8c), and the tangential velocities (fig. 8d) all show significant $2\Delta r$ components.

Again, however, these small-scale features certainly are not dominant. In the pressure profile (fig. 10), for example, a distinct large-scale pattern clearly stands out from the small-scale oscillations. By eight hours (fig. 9), a drastic change in the character of the system has taken place. This change reflects the fact that gravitational instability is no longer of importance. The lapse rate in the ascending air has become statically neutral except in the very high troposphere where it continues to be unconditionally stable. The combined effects of baroclinic instability (see fig. 9c), weak inertial stability in the low layers, and some inertial instability in the high troposphere (see fig. 9d) are now the important factors. The column of ascending air (fig. 9a) has become, without question, a large-scale feature. A narrow column of intense descent is found at the vortex center. The small-scale features in the temperature field (fig. 9c), the field of v_θ (fig. 9d), and the sea level pressure profile (fig. 10) have, for the most part, vanished. The radial velocities (fig. 9b) show deep layers of intense inflow and outflow. These radial velocities, as well as the subsidence at the vortex center, are, of course, much too intense to be realistic. The central pressure of the system (fig. 10) is now 945 mb. and the maximum v_θ (fig. 9d) is 55 m. sec.$^{-1}$ Note that the region of this maximum has migrated in toward the storm center.

Figure 11 shows semi-logarithmic, time-plots of the maximum w and the maximum v_θ. We note that between one and five hours, v_θ and w both tend to follow exponential growth laws. Over this period, the growth rate for w is 2.4×10^{-4} sec.$^{-1}$ This growth rate agrees fairly well (see, for example, [11]) with what one would expect from linear theory for a barotropic base state with gravitational instability at a wavelength of about 200 km. The growth rate for v_θ, between one and five hours, is 5.3×10^{-5} sec.$^{-1}$ The difference between these growth rates would seem to indicate that nonlinear and baroclinic mechanisms play a much more important role in determining v_θ than in determining w. It would also seem that the departure from the exponential growth law, which takes place after five hours, indicates a fundamental change in the dominant physical mechanisms.

In comparison to real hurricanes, Experiment II shows deepening which is much too rapid; the central pressure decreased 55 mb. in eight hours. Also, the meridional circulation is much too intense; it is highly doubtful that outflow of 35 m. sec.$^{-1}$ or subsidence on the order of 200 cm. sec.$^{-1}$ would ever be found in a real storm. To assess the effect of friction on the development of the system, the experiments described by table 1 were performed. Each of these calculations was carried to five hours.
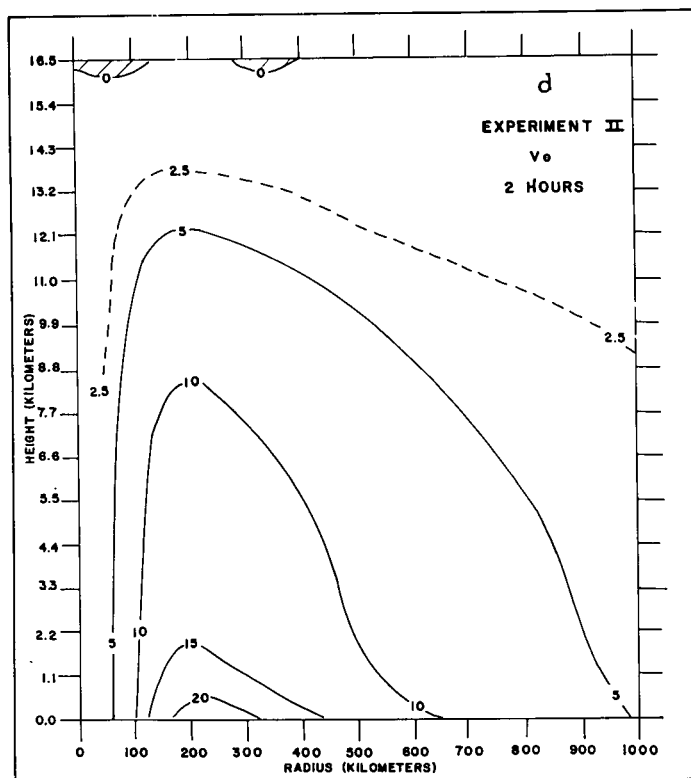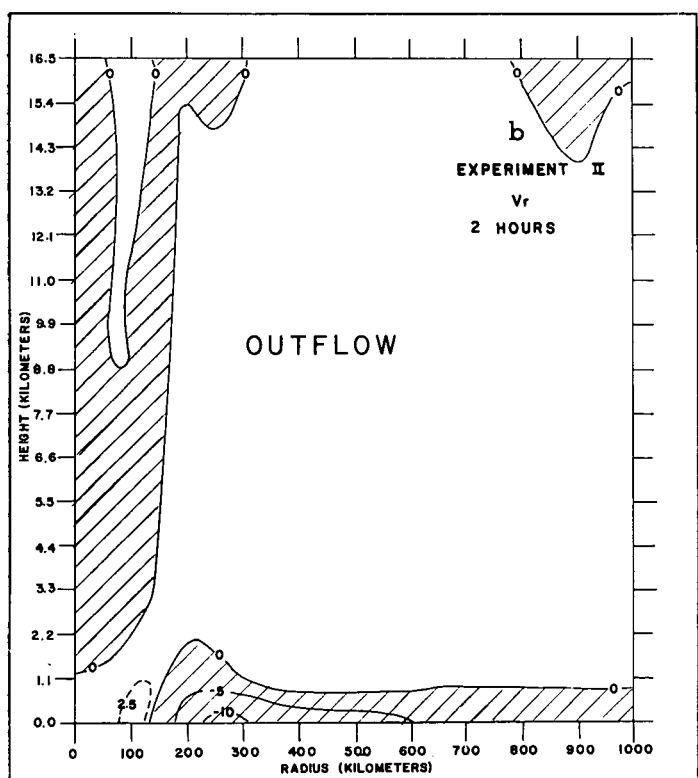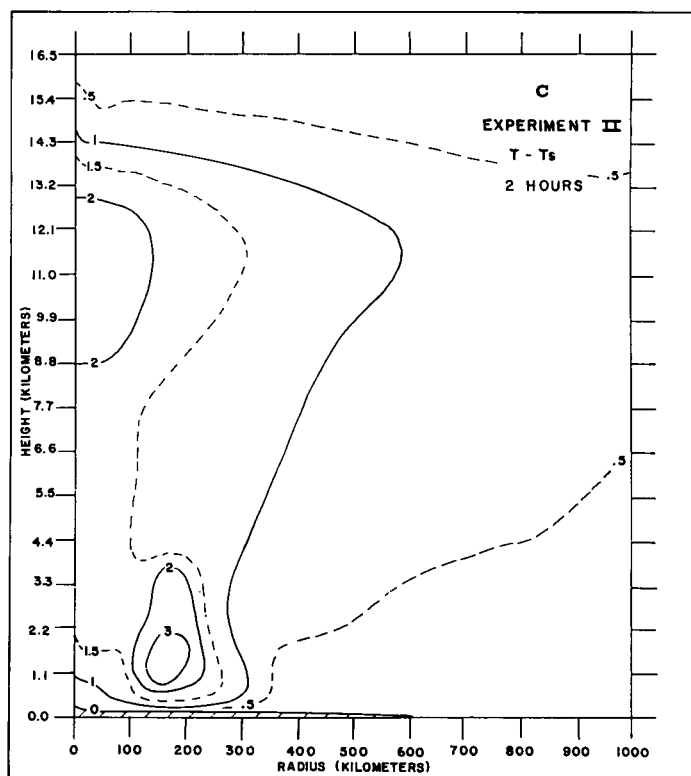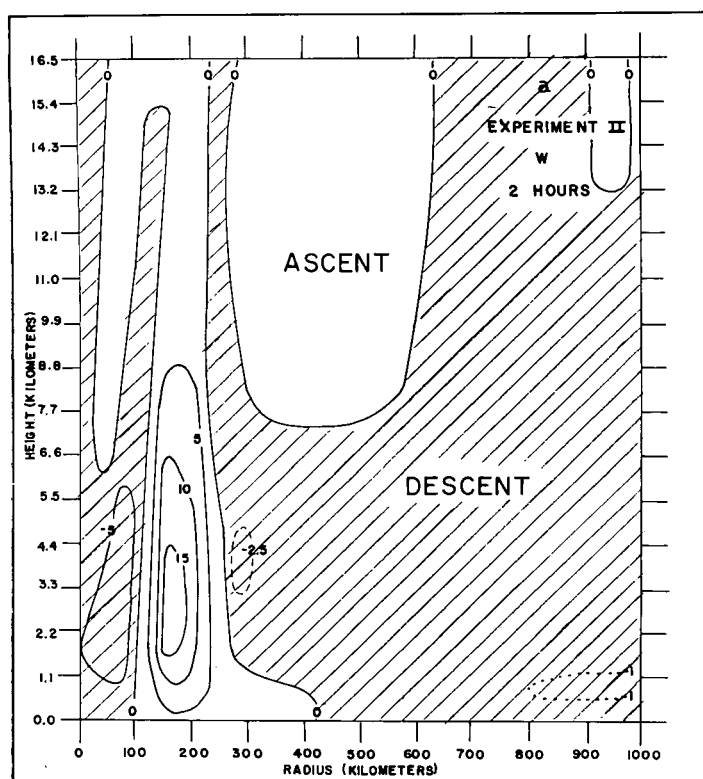
FIGURE 6.—Experiment II, two hours, (a) vertical velocity (cm. sec.$^{-1}$), (b) radial velocity (m. sec.$^{-1}$), (c) temperature anomaly ($T-T_s$) in °C., (d) tangential wind (m. sec.$^{-1}$).
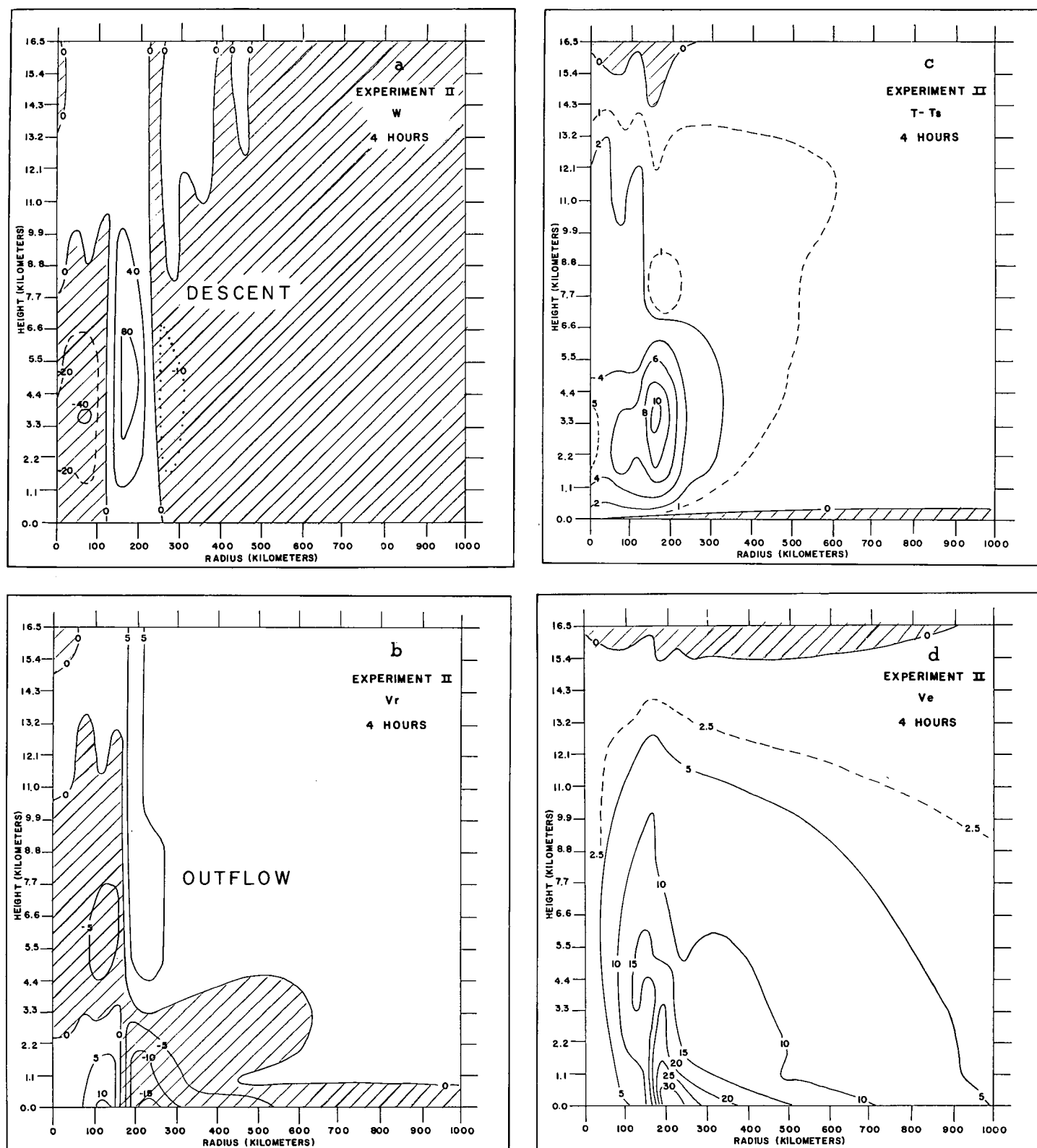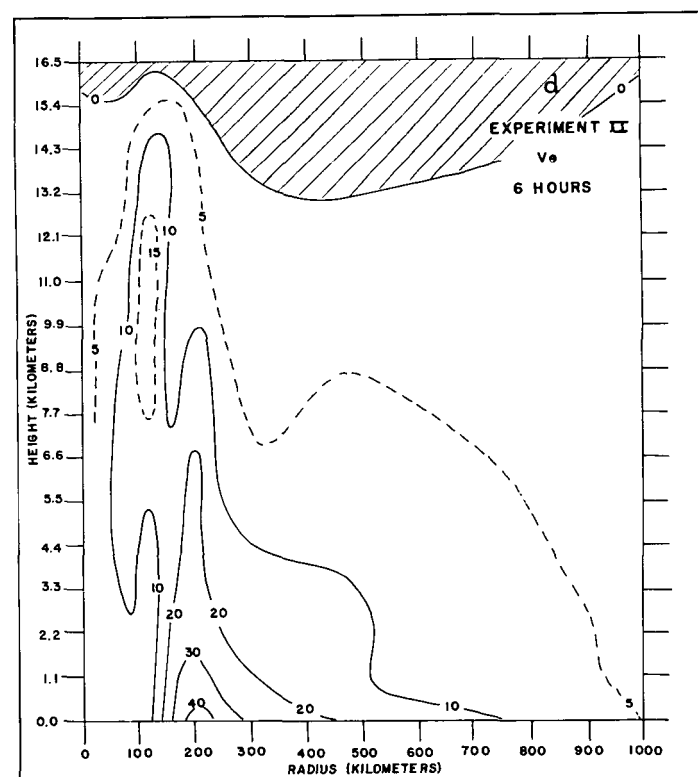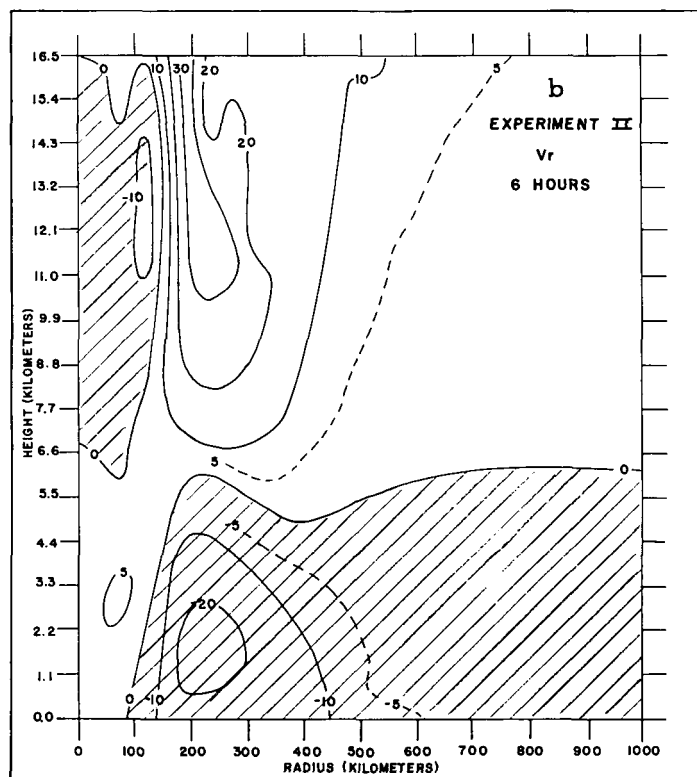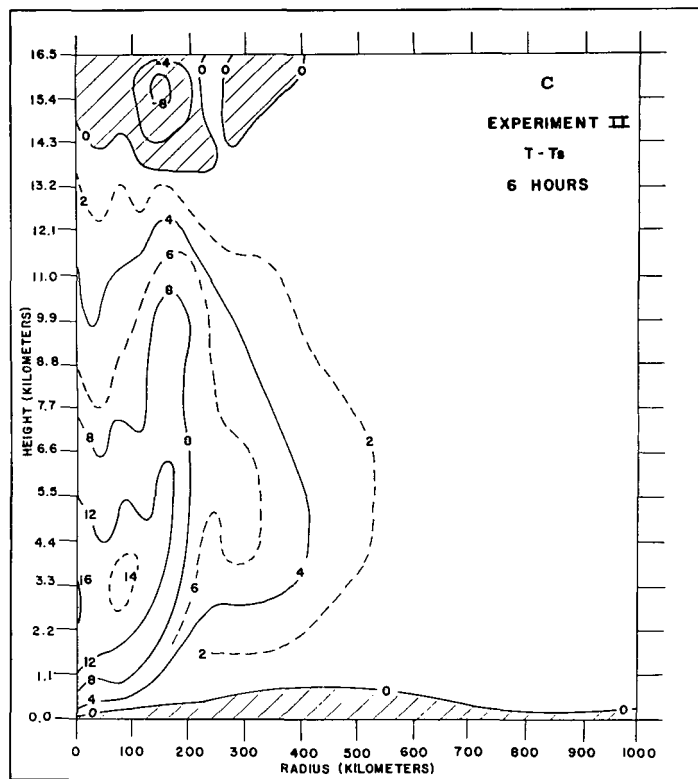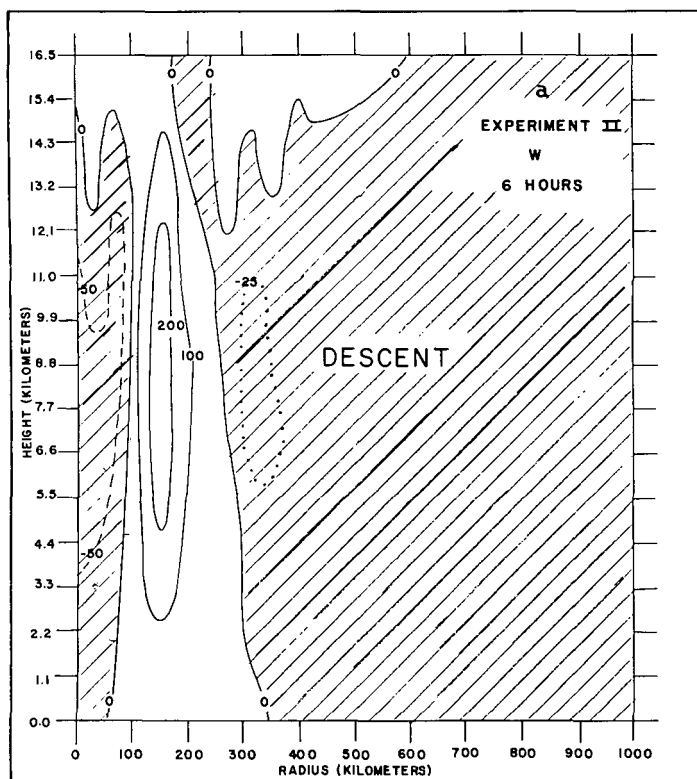
FIGURE 7.—Experiment II, four hours.
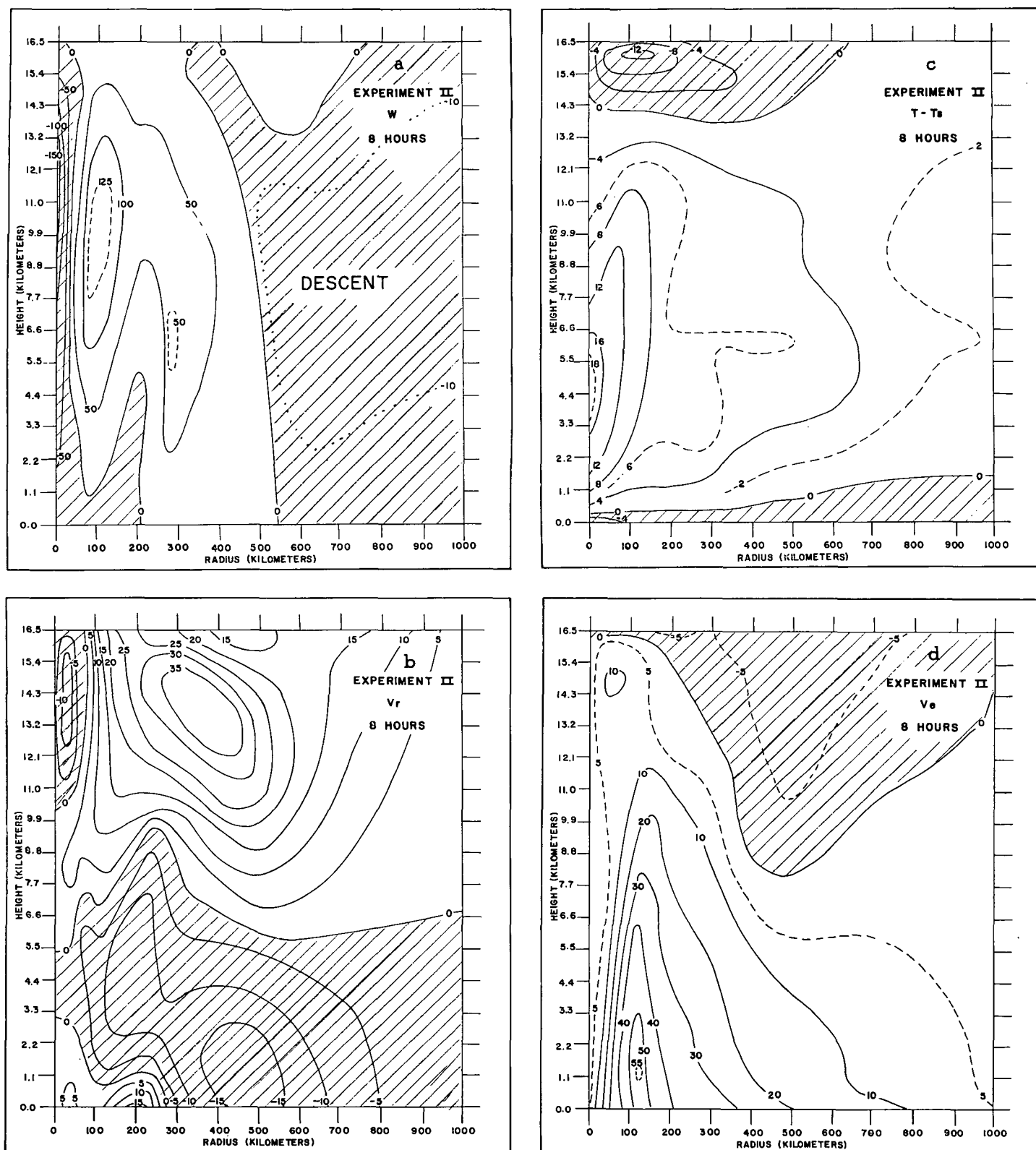
FIGURE 8.—Experiment II, six hours.

FIGURE 9.—Experiment II, eight hours.

TABLE 1.—*Description of Experiments III, IV, V, and VI*

	C_D	$K_z(z=0)$	$K_z(z=h)$	K_H	Initial $(T-T_{sea})$
	$(\times 10^{-3})$	(m.²/sec.⁻¹)		(m.²/sec.⁻¹)	
Experiment III	2.5	10	0	0	0
Experiment IV	2.5	10	0	5×10^4	0
Experiment V	2.5	10	0	1×10^5	0
Experiment VI	2.5	10	0	5×10^5	0

Experiment III includes surface friction, air-sea exchange of sensible heat (with this quantity zero at the initial instant), and vertical mixing of heat and momentum. Characteristic features of the system after five hours are summarized by table 2. For Experiment III, we see that the meridional circulation is even more intense than that of Experiment II; characteristic radial and vertical velocities are 2 to 3 times greater. The configurations of the flow and thermal patterns in Experiments II and III are, however, about the same with the exception that the main ascending current is slightly wider in Experiment III and the tangential wind develops a shallow layer of weak, frictionally retarded winds close to sea level. The maximum tangential wind in Experiment III is about 9 m. sec.⁻¹ smaller than that of Experiment II. In response to the stronger meridional circulation, the temperature anomalies developed in Experiment III are as much as 7° C. greater than those of Experiment II. Pressure profiles for Experiment III show small-scale oscillations similar to those of Experiment II. After five hours, the lowest pressure is 19 mb. lower than that of Experiment II.

Experiment IV differs from Experiment III only in the inclusion of lateral mixing terms with $K_H=5\times10^4$ m.² sec.⁻¹ Again, Experiment IV gives flow and thermal patterns whose configurations are very much like those obtained from Experiments II and III. For the most part, the lateral mixing terms tend to counterbalance the vertical mixing terms. After five hours, the lowest sea level pressure in Experiment IV is about halfway between those of Experiments II and III. The pressure profiles show small-scale oscillations. The meridional circulation is not as intense as in Experiment III but more intense than in Experiment II. The maximum v_θ is not significantly different from that of Experiment III.
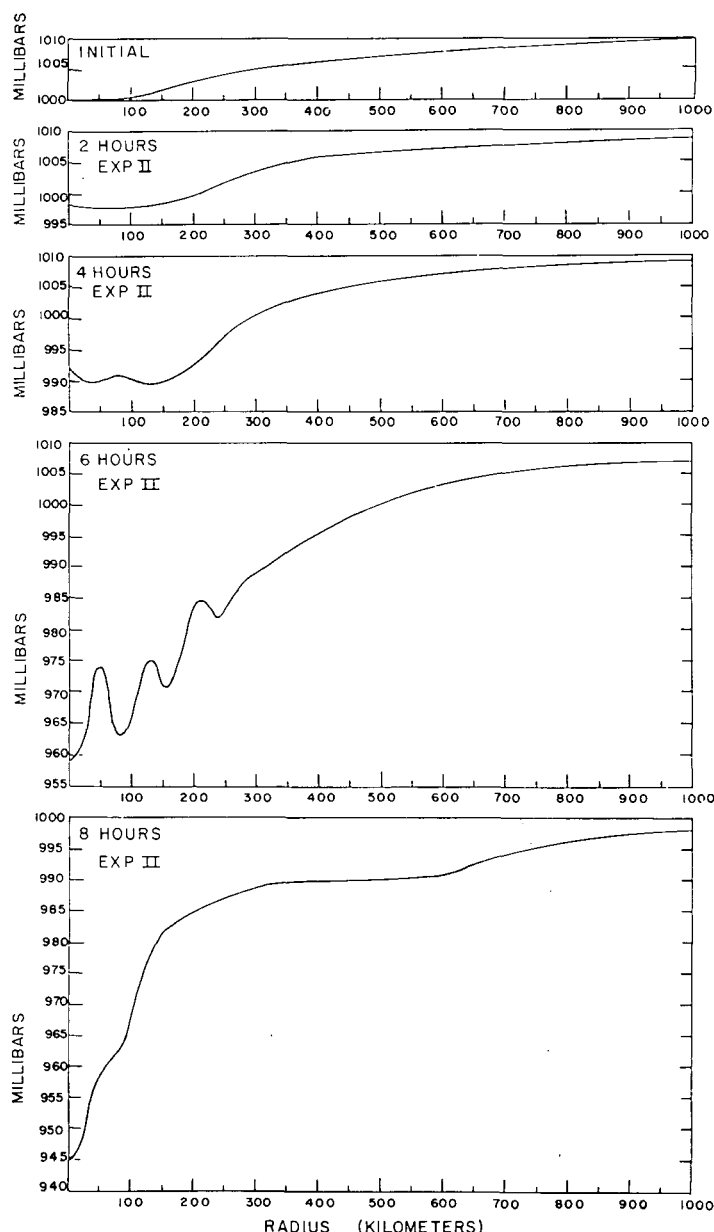

FIGURE 10.—Experiment II, sea level pressure as a function of radius at two-hour intervals.

TABLE 2.—*Characteristic properties of Experiments II, III, IV, V, and VI after five hours.*

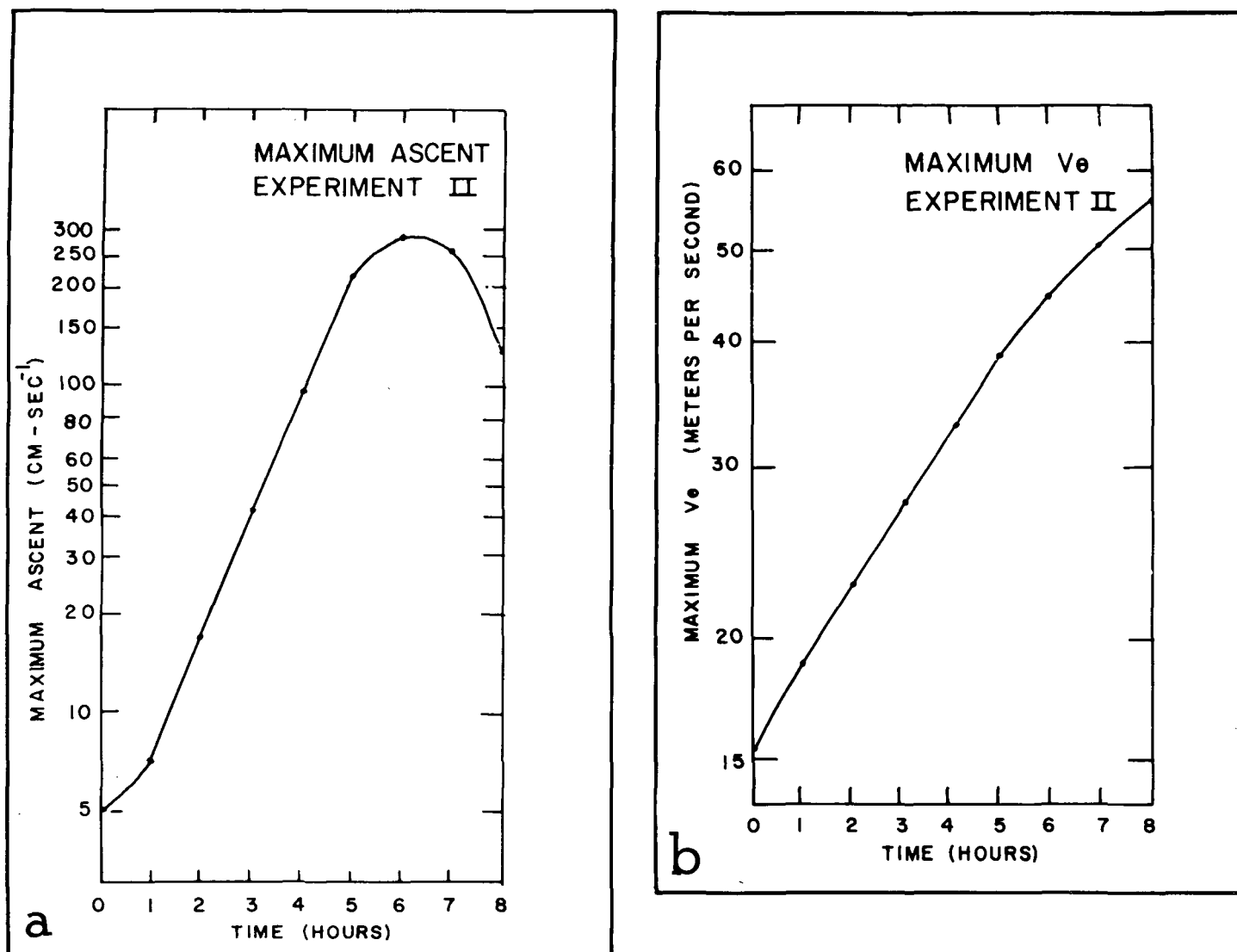|	Maximum tangential wind (m. sec.⁻¹)	Lowest pressure (mb.)	Maximum ascent (cm. sec.⁻¹)	Maximum descent (cm. sec.⁻¹)	Maximum outflow (m. sec.⁻¹)	Maximum inflow (m. sec.⁻¹)	Maximum $(T-T_s)$ at $r=0$ (°C)	Maximum $(T-T_s)$ in main ascending column (°C)
Experiment II	39.4	979	210	−82	17.8	−18.2	10.4	12.9
Experiment III	30.3	960	379	−190	50.2	−42.8	17.2	14.8
Experiment IV	27.9	971	305	−136	35.8	−38.9	14.5	14.4
Experiment V	25.9	977	147	−97	24.8	−35.4	12.3	13.4
Experiment VI	17.3	994	47	−6	6.3	−19.5	8.2	only one maximum

FIGURE 11.—Experiment II, (a) maximum ascent (cm. sec.$^{-1}$) as a function of time, (b) maximum tangential wind (m. sec.$^{-1}$) as a function of time.

In Experiment V, K_H was increased to 10^5 m.^{2} sec.$^{-1}$ No other parameters were varied. The configurations of the flow and thermal patterns are, again, very much like those of Experiment II. Comparisons between Experiments IV and V show the maximum tangential winds and the lowest sea level pressures to be about the same in the two experiments. Vertical motions in Experiment V are, however, substantially less than in Experiment IV. The maximum outflow at the upper levels is about 10 m. sec.$^{-1}$ weaker in Experiment V than in Experiment IV. The maximum inflow in the low layers is about the same as that of Experiment IV.

For Experiment VI, K_H was increased to 5×10^5 m.^{2} sec.$^{-1}$ Although Experiments II, III, IV, and V produce flow and thermal patterns which are remarkably similar, Experiment VI gives vastly different results. This experiment shows no hint of disturbances on the scale of $2\Delta r$. After five hours, vertical motions and upper-level outflow are considerably weaker than in the previous experiments. The maximum v_θ and the lowest sea level pressure vary only slightly from their initial values. Note that the maximum low-level inflow and the maximum v_θ are approximately equal. Experiment VI was continued to 10 hours. The tendency to produce maximum v_θ and maximum inflow of approximately the same magnitude continued during this time. At 10 hours, both of these quantities are about 30 m. sec.$^{-1}$ In summary, $K_H = 5 \times 10^5$ m.^{2} sec.$^{-1}$ eliminates the short-wave components and slows the development of the meridional circulation. Nevertheless, the meridional circulation ultimately does become too strong. Furthermore, $K_H = 5 \times 10^5$ m.^{2} sec.$^{-1}$ tends to produce a system in which the kinetic energy, at
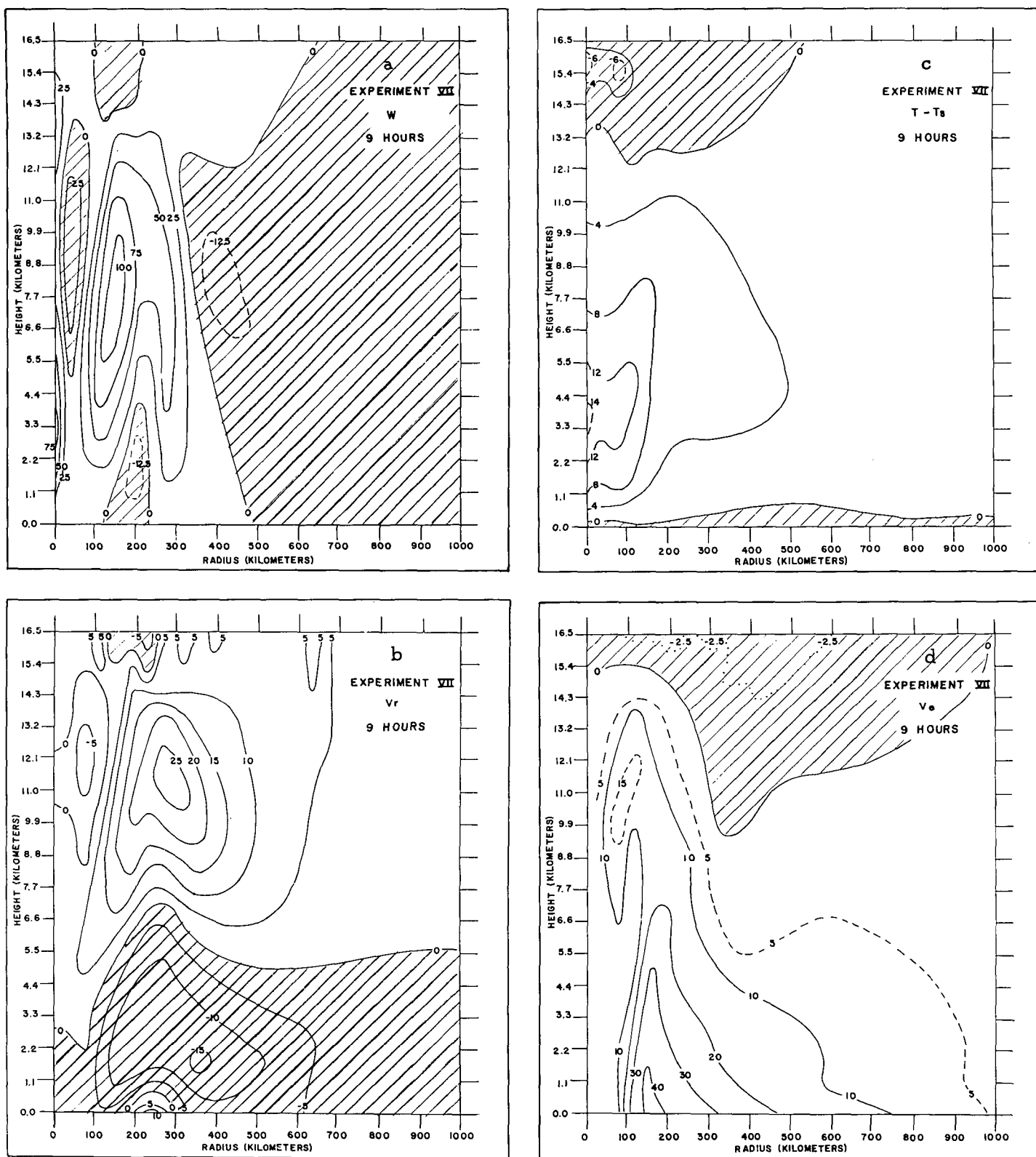
FIGURE 12.—Experiment VII, nine hours, (a) vertical velocity (cm. sec.⁻¹), (b) radial velocity (m. sec.⁻¹), (c) temperature anomaly $(T-T_s)$ in °C., (d) tangential wind (m. sec.⁻¹).
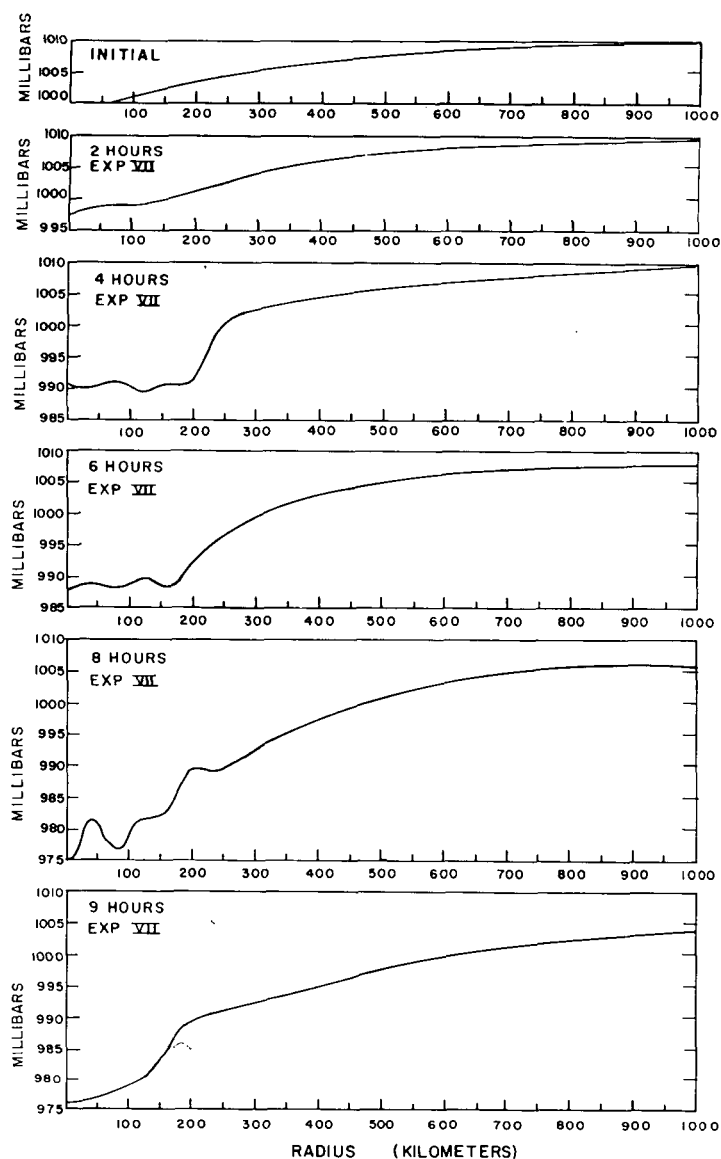
FIGURE 13.—Experiment VII, sea level pressure as a function of radius at various times.

low levels, is distributed about equally between the rotational and divergent components of the wind.

Our last integration, designated Experiment VII, was identical to Experiment II with the exception that the wet static stability, $(\partial\theta/\partial z)+(\gamma L/\phi)\,(\partial q_s/\partial z)$ in equation (16), was multiplied by 0.75 when w was positive. The factor of 0.75 attempts to take into account effects (such as the evaporation of falling rain) which prevent the occurrence of the pseudo-adiabatic process in nature. The evolution given by Experiment VII, with a lag of a few hours, is very much like that given by Experiment II.

The state of the vortex after nine hours of Experiment VII is shown by figure 12. We will compare these results to those of Experiment II at eight hours. The large-scale aspects of the two vertical motion patterns (figs. 9a and 12a) are strikingly similar. Strongest ascent in Experiment VII is 116 cm. sec.$^{-1}$, compared to 131 cm. sec.$^{-1}$ in Experiment II. In Experiment VII, ascent as great as 78 cm. sec.$^{-1}$ occurs at the vortex center. This is in contrast to intense subsidence found here in Experiment II. Experiment VII does show some fairly strong subsidence between 40 and 80 km. In this region, downward vertical motions are as large as 46 cm. sec.$^{-1}$. As a result of the continued presence of conditional instability in Experiment VII which, in turn, is the result of the weaker ascent and lower rate of heating in this experiment, the main rising current is considerably narrower than in Experiment II.

The radial motion patterns (figs. 9b and 12b) for Experiments II and VII are quite similar. Upper-level outflow in Experiment VII is as large as 25 m. sec.$^{-1}$. The patterns of temperature anomaly (figs. 9c and 12c) are also similar, the intensity being somewhat less for Experiment VII.

The time lag between Experiments II and VII is very clear in the tangential velocity fields. v_θ, after nine hours of Experiment VII (fig. 12d), shows an extremely close resemblance to its value at six hours in Experiment II (fig. 8d). The pressure profiles for Experiment VII are shown by figure 13. As has been the case with all experiments, development in Experiment VII takes place much too rapidly and the meridional circulation is much too strong.

7. SUMMARY AND CONCLUSIONS

In Experiment II, a vortex which was initially fairly weak intensified and surpassed hurricane intensity by a considerable margin. This intensification occurred much too rapidly and the meridional circulation which evolved was much too intense. When ground friction and vertical mixing were added, the meridional circulation became even more intense and the pressure field deepened even more rapidly. Lateral mixing tended to slow down the development of the system. However, as shown by Experiment VI, this provided only a temporary delay in the generation of an unacceptably intense meridional circulation.

It appears that the over-zealous intensification of the vortex is due to a basic flaw in the design of the experiment. One obvious source of this difficulty is the assumption that all ascending air is saturated with water vapor. This, of course, can be remedied by including an equation of continuity for water vapor. A second possible difficulty is the requirement that the upper boundary be rigid and isobaric. If the tropopause over the storm center were allowed to rise as the system develops, pressures would drop less rapidly, the development would proceed more slowly, and the meridional velocities might not reach the enormous values obtained in the experiments described above.

REFERENCES

1. A. Eliassen, "Slow Thermally or Frictionally Controlled Meridional Circulations in a Circular Vortex," *Astrophysica Norvegica*, vol. 5, No. 2, May 1952, pp. 19–60.

2. A. Eliassen, "Remarks on the Problem of Long Range Weather Prediction," in *Dynamics of Climate*, Pergamon Press, New York, 1960, pp. 37–43.

3. A. Eliassen, "On the Formation of Fronts in the Atmosphere," in *The Atmosphere and Sea in Motion* (the Rossby Memorial Volume), Rockefeller Institute Press, New York, 1959, pp. 425–439.

4. M. A. Estoque, "Vertical and Radial Motions in a Tropical Cyclone," *Tellus*, vol. 14, No. 4, Nov. 1962, pp. 394–402.

5. A. Kasahara, "A Numerical Experiment on the Development of a Tropical Cyclone," *Journal of Meteorology*, vol. 18, No. 3, June 1961, pp. 259–282.

6. A. Kasahara, "The Development of Forced Convection Caused by the Released Latent Heat of Condensation in a Hydrostatic Atmosphere," *Technical Report* No. 14, Contract Cwb–9941, Department of Meteorology, The University of of Chicago, 1960, 42 pp.

7. A. Kasahara, "A Study of Stability of Thermally Driven and Frictionally Controlled Symmetrical Motions with Application to the Mechanism for Development of Tropical Cyclones," *Technical Report* No. 16, Contract Cwb–9941, Department of Meteorology, The University of Chicago, 1961, 64 pp.

8. H. L. Kuo, "Forced and Free Axially-Symmetric Convection Produced by Differential Heating in a Rotating Fluid," *Journal of Meteorology*, vol. 13, No. 6, Dec. 1956, pp. 521–527.

9. H. L. Kuo, "On the Initiation of Tropical Depressions and Convection in a Conditionally Unstable Atmosphere," *National Hurricane Research Project Report* No. 40, 1960, 46 pp.

10. H. L. Kuo, "Mechanism Leading to Hurricane Formation," in "Proceedings of the Second Technical Conference on Hurricanes," *National Hurricane Research Project Report* No. 50, 1962, pp. 277–283.

11. D. K. Lilly, "On the Theory of Disturbances in a Conditionally Unstable Atmosphere," *Monthly Weather Review*, vol. 88, No. 1, Jan. 1960, pp. 1–17.

12. D. K. Lilly, "A Proposed Staggered Grid System for Numerical Integration of Dynamic Equations," *Monthly Weather Review*, vol. 89, No. 3, Mar. 1961, pp. 59–65.

13. B. I. Miller, "On the Momentum and Energy Balance of Hurricane Helene (1958)," *National Hurricane Research Project Report* No. 53, 1962, 19 pp.

14. B. I. Miller, "On the Filling of Tropical Cyclones Over Land," *National Hurricane Research Project Report*, No. 66 (in press).

15. H. Riehl and J. S. Malkus, "Some Aspects of Hurricane Daisy, 1958," *National Hurricane Research Project Report* No. 46, 1961, 53 pp.

16. R. D. Richtmyer, *Difference Methods for Initial Value Problems*, Interscience Publishers, New York, 1957, 238 pp.

17. S. L. Rosenthal, "On the Problem of the Diagnostic Calculation of Vertical and Radial Motions in a Wet Vortex," *Monthly Weather Review*, vol. 91, No. 9, Sept. 1963, pp. 453–464.

18. S. Syono, "A Numerical Experiment of the Formation of Tropical Cyclones," in *Proceedings of the International Symposium on Numerical Weather Prediction in Tokyo*, The Meteorological Society of Japan, Tokyo, 1962.

19. M. Yanai, "Dynamical Aspects of Typhoon Formation," *Journal of Meteorological Society of Japan*, vol. 39, No. 5, Oct. 1961, pp. 282–309.